https://doi.org/10.5194/esd-2023-10
Preprint. Discussion started: 25 April 2023

Earth System Dynamics
Discussions

Low confidence in multi-decadal trends of wind-driven upwelling across the Benguela upwelling system due to internal climate variability

Mohammad Hadi Bordbar, Volker Mohrholz and Martin Schmidt

Leibniz Institute for Baltic Sea Research Warnemünde (IOW), Rostock, Germany

Correspondence to: Mohammad Hadi Bordbar (hadi.bordbar@io-warnemuende.de; Ocean.Circulation@gmail.com)

Abstract. Like other Eastern Boundary Upwelling Systems, the upwelling near the southwest African coasts is primarily alongshore-wind-driven, whereas it is controlled mainly by the wind stress curl farther offshore. The surface wind regime across the Benguela Upwelling System is strongly related to the South Atlantic Anticyclone that is believed to migrate poleward in response to anthropogenic global warming. Here, we investigate multi-decadal changes of the South Atlantic Anticyclone and their impacts on the cross-shore integral of wind-driven coastal upwelling, the wind stress curl-driven, and total upwelling across the Benguela Upwelling System. Even though the detailed structure of surface wind over the coastal zone matters for both local wind-driven coastal upwelling and wind stress curl-driven upwelling, we show that it is not of major importance for the total amount of upwelled water. We found a robust connection between the Anticyclone intensity and the integrated wind stress curl-driven and total upwelling. However, this connection for the wind-driven coastal upwelling is weak. With more signatures during austral winter, the upwelling in the equatorward portion of the Benguela Upwelling System is significantly affected by the anticyclone intensity. In contrast, the poleward portion is also influenced by the meridional position of the anticyclone. The multi-decadal trend in the sea level pressure across the South Atlantic renders a considerable heterogeneity in space. However, this trend features a small signal-to-noise ratio and can be obscured by internal climate variability. This view is further supported by a multi-decadal trend in the integrated coastal and wind-stress-curl-driven upwelling in several upwelling cells, which hardly depict any significant systematic changes.

1 Introduction

Human-induced changes in the Earth's climate system have raised enormous concern for the future of marine ecosystems across the major Eastern Boundary Upwelling Systems (EBUS) with considerable resources of the world's pelagic fish (Pauly and Christensen, 1995; Rykaczewski et al., 2015; Abraham et al. 2021). At the same time, modes of natural climate variability, which span a broad range of timescale exert profound impacts on the functioning of the EBUS marine ecosystems (Jarre et al., 2015b; Rykaczewski et al., 2015). These modes are resulted from nonlinear climate dynamics and modulate the ocean-atmosphere heat, mass, and momentum exchanges on the regional or even global scale.

The Benguela Upwelling System (BUS) is located in the eastern margin of the subtropical South Atlantic and extends from the Cape of Good Hope in South Africa to southern Angola (Shannon 1985). The BUS is one of the world's most productive marine ecosystems with several distinct upwelling cells (Johnson, 1976; Kainge et al., 2020; Jarre et al., 2015b). In each cell, the wind stress and its spatial heterogeneity are major upwelling drivers (Fennel,

https://doi.org/10.5194/esd-2023-10
Preprint. Discussion started: 25 April 2023

1999). Near the coast, upwelling is proportional to the alongshore wind stress and associated with offshore-directed transport. This type of upwelling is referred to as coastal upwelling. It is vigorous but confined to narrow coastal zones (~30 km wide). Farther offshore, the Ekman transport shows a relatively weak divergence resulting in an upward (downward) velocity that is proportional to the local negative (positive) wind stress curl. This source of upwelling is termed the wind-stress-curl-driven (WSCD) upwelling. Typically, the WSCD upwelling is much weaker than the coastal upwelling, but extends over a broader area (Fennel, 1999; Bordbar et al., 2021). Given the different characteristics of these two sources of upwelling, they favor different pelagic food webs (Rykaczewski et al., 2008; Lamont et al., 2019).

A steep drop-off in the alongshore wind towards the coast often occurs near the coastal zones of the BUS, driving an intensified nearshore WSCD upwelling. From an analytical theory of upwelling and results of a state-of-the-art ocean circulation model, Bordbar et al. (2021) showed that the volume of upwelled water due to the coastal offshore transport and the wind stress curl is almost in the same order of magnitude in the BUS.

Feistel et al. (2013) showed that Namibian shelf upwelling events are closely connected to the sea level pressure (SLP) changes in St. Helena Island (5.7°W, 15.95°S). Based on observed surface air temperature, SLP, and precipitation, they introduced the St. Helena Island Climate Index to describe interannual anomalous coastal warm and cold events, known as Benguela Niños and Niñas.

Surface wind across the Namibian shelf is affected by a northward atmospheric low-level jet, which is known as the Benguela low-level coastal jet. The signatures of this low-level jet are more prominent at about 17°S and 25°S-30°S, which coincide with Kunene and Lüderitz upwelling cells, respectively (Patricola and Chang, 2017). In general, the atmospheric flow across the subtropical South Atlantic is largely influenced by the subtropical South Atlantic Anticyclone (SAA) (Feistel et al., 2003; Richter et al., 2008; Lamont et al., 2018). In the equatorward part of the BUS (nBUS), the surface wind persists year-round and is approximately proportional to the cross-shore SLP gradient between the SAA and the Angola-Kalahari low-pressure system (Feistel et al., 2003). In contrast, the wind in the poleward portion of the BUS undergoes strong seasonal variations (sBUS, Shannon 1985; Shannon and Nelson 1996). Lamont et al. (2018) found the total amount of upwelled water associated with coastal offshore transport in the nBUS is affected by the strength of the SAA. In contrast, enhanced coastal offshore transport was observed in the sBUS when the SAA shifted to the south.

The SLP variability across the south Atlantic is affected by natural modes of climate variability. The Southern Annular Mode (SAM) is the dominant mode of climate variability in the extratropical southern hemisphere and is expressed as a ring-shaped structure of the SLP anomalies around the polar latitudes with fluctuations ranging from synoptic to decadal timescales (Gilett et al. 2006; Wachter et al. 2020; Fogt and Marshall 2020). The positive phase of the SAM is defined as a positive anomaly in the meridional pressure gradient between relatively low pressure located over the southern hemisphere polar latitude and high pressure at the mid-latitudes. Over recent decades, the SAM has undergone a positive trend (Wachter et al. 2020). The El Niño Southern Oscillation, the Atlantic Niño, the interdecadal Pacific Oscillation, and the Atlantic Multidecadal variability are examples of internal modes of climate variability affecting the South Atlantic climate (Shannon et al., 1986; Kidson, 1988; Gillett et al., 2006; Rouault & Tomety, 2022).

The future of wind-driven upwelling across the subtropical eastern edge of major ocean basins inspired several studies (Bakun, 1990; Narayan et al., 2010; Sydeman et al., 2014; Rykaczewski et al., 2015). Using observational wind

https://doi.org/10.5194/esd-2023-10
Preprint. Discussion started: 25 April 2023

products over the last decades, Lamont et al. (2018) and Abrahams et al. (2021) found a significant downward trend in the number of offshore-directed coastal Ekman transport events across the nBUS, whereas it underwent an upward trend in the sBUS. The majority of climate models project an acceleration (slight deceleration) of upwelling favorable winds over the poleward (equatorward) margins of the EBUS (Rykaczewski et al., 2015; Bonino et al., 2019). However, these simulated trends were less prominent in the BUS (Rykaczewski et al., 2015). These studies were inspired by a conceptual hypothesis raised by Bakun (1990), suggesting coastal upwelling would strengthen in response to anthropogenic global warming. The basic premise of this hypothesis comes back to the intensified cross-shore SLP gradient associated with excess warming over the landmass relative to adjacent ocean waters. During summer, when solar radiation reaches its seasonal maximum, the cross-shore SLP contrast enhancement is expected to be more severe.

Several limiting factors hinder the assessment of Bakun's hypothesis in the BUS. First, observations over this part of the South Atlantic are sparse in time and space. Second, climate models, widely used for past and future climate changes, suffer from a long-standing sea surface temperature (SST) bias over the southeast Atlantic with considerable impacts on the regional atmospheric flow (Sun et al., 2017; Li et al., 2020). Third, changes associated with internal modes of climate variability overshadow the signature of the externally-forced trends (Bordbar et al., 2015; Tim et al., 2015; Latif et al., 2016; Bonino, 2019; Polonsky and Serebrennikov, 2021). For example, it is unclear how long it would take for incremental changes in the coastal wind to emerge from the background fluctuations associated with internal climate variability. One should keep in mind that the characteristics of the internal climate variability (i.e., magnitude, frequency) might change in response to enhanced radiative forcing.

Hence, it remains controversial whether the mechanism suggested by Bakun is the dominant factor for upwelling changes across the BUS. The major concern is that the WSCD upwelling is of great importance for marine ecosystems across the BUS, but neither its mechanism nor its response to global warming is considered in Bakun's hypothesis. It is important to bear in mind that the coastal and the WSCD upwelling do not necessarily undergo identical fluctuations and are sometimes out of phase (Rykaczewski et al., 2008; Bordbar et al., 2021). To understand the relation of the SAA with the coastal and the WSCD upwelling in the BUS, we assess their linkage from the ERA5 products over 1979-2021. We discuss the robustness of the long-term trends in the SAA, and the SLP over the South Atlantic. Furthermore, we assess the long-term changes in the probability distribution of coastal and WSCD upwelling in several coastal upwelling cells across the BUS in 1979-2021.

2 Data and methods

The hourly SLP and surface wind vectors from the European Centre for Medium-Range Weather Forecasts (ECMWF) ERA5 reanalysis for 1979-2021 (43 years) are analyzed in this study (Hersbach et al., 2018). The spatial resolution of the datasets is 0.25°x0.25° regular grid. The daily and monthly averages are computed from the hourly values. To validate ERA5 wind data, we utilize satellite-derived daily ASCAT datasets covering the period of 2007-2021 (Ricciardulli and Wentz, 2016). We additionally use the in situ measurements in St. Helena Island (5.7°W-15.95°S) with a long-term record from 1893 to the present (Feistel et al., 2003). In general, ERA5 shows a good agreement with ASCAT and St. Helena Island SLP (Supplementary Info; Fig. S1-4). This is consistent with the findings of Belmonte Rivas and Stoffelen (2019).

To compute the wind stress, τ, we use a bulk formula as

https://doi.org/10.5194/esd-2023-10
Preprint. Discussion started: 25 April 2023

$$\vec{\tau} = C_d \rho_a U_{10} \vec{U}_{10}, \tag{1}$$

where U_{10}, $\vec{U}_{10}$, ρ_a and C_d represent the wind velocity magnitude (m/s) at 10-meter height above the sea surface, the surface wind velocity, surface air density (kg/m^3), and the dimensionless neutral drag coefficient, respectively. ρ_a and C_d are taken as constant values at 1.23 kg/m^3 and 0.0013 assuming neutral stability in the atmospheric boundary layer (Gill 1982).

The Ekman wind-driven ocean current theory is broadly used to describe the flow at the ocean surface. It is based on the balance between the vertical flux of horizontal momentum associated with wind stress, τ, and the Coriolis force (Ekman 1905). In this theory, the vertically integrated zonal (U_E) and meridional (V_E) volumes transport (m^2/s) per unit length are expressed as:

$$U_E = \frac{\tau_y}{\rho_w f} \qquad and \qquad V_E = \frac{-\tau_x}{\rho_w f}, \tag{2}$$

where ρ_w and f are the density of seawater and Coriolis parameter, respectively. f is negative in the Southern Hemisphere. The divergence of the Ekman transport in the open ocean, which is proportional to the wind stress curl, is related to a vertical velocity in the water column. The WSCD upwelling in the f-plane approximation (i.e., invariant f) (Johnson 1976; Fennel and Lass 2007) is:

$$w_{curl} = \frac{1}{\rho_w f}\left(\frac{\partial \tau_y}{\partial x} - \frac{\partial \tau_x}{\partial y}\right). \tag{3}$$

Since the orientation of southwest African coastlines is almost in the meridional direction and the major component of the wind stress orients meridionally, we take the meridional component as the alongshore wind stress (Fennel 1999; Bordbar et al., 2021). In this way, the major element of the Ekman transport is the zonal component, taken as a good approximation for the cross-shore component. The major contributor to the wind stress curl is the zonal variation of the meridional wind stress. Hence, the WSCD (i.e., w_{curl}) upwelling can be approximated as:

$$w_{curl} \approx \frac{1}{\rho_w f}\left(\frac{\partial \tau_y}{\partial x}\right). \tag{4}$$

The balance between wind stress and Coriolis force from the Ekman transport, as the primary assumption of the Ekman dynamics, is disturbed near the coast. A downwind swift ocean current, known as coastal jet, forms near the coast (Yoshida 1959, Fennel 1999). In addition to the cross-shore directed Ekman transport another cross-shore directed transport component emerges, referred to as U_c. This way, the boundary condition of no flow through the coast is satisfied by the total cross-shore transport, $U_E + U_c$. The coastal upwelling associated with the divergence of the total cross-shore directed transport is confined to a coastal stripe with a width of about the first baroclinic Rossby radius of deformation (R_1) (Yoshida 1959, Fennel 1999). We approximate the coastal upwelling velocity (w_{coast}) as suggested in Bordbar et al. (2021) as:

$$w_{coast} = \frac{-2\tau^y(x=0)}{f\rho_w}\frac{e^{\frac{2x}{R_1}}}{R_1}. \tag{5}$$

Here, x and τ^y are the distance to the coast, and meridional wind-stress, respectively. Note that x is negative in the westward offshore direction. w_{coast} is reduced sharply with coastal distance and is negligible beyond the coastal distance of R_1.

https://doi.org/10.5194/esd-2023-10
Preprint. Discussion started: 25 April 2023

Earth System Dynamics Discussions

The WSCD upwelling velocity, w_{curl}, is typically one order of magnitude smaller than the coastal upwelling velocity, w_{coast}. In turn, the coastal upwelling is localized within a narrow coastal stripe of a few 10km width. In contrast, w_{curl} extends from the coast to a few 100km offshore. For our investigation, we consider the cross-shore directed (i.e., zonal) integral of both upwelling contributions, which may be both of similar magnitude. For a location, x, in a distance from the coast much larger than R_1, (i.e., $|x| \gg R_1$), this integral reads:

$$W_{total}(x) = \int_x^0 dx'(w_{curl} + w_{coast}) \approx -\left(\frac{\tau^y(x)}{f\rho_w} - \frac{\tau^y(x=0)}{f\rho_w}\right) - \frac{\tau^y(x=0)}{f\rho_w} = -\frac{\tau^y(x)}{f\rho_w} = -U_E(x). \quad (6)$$

The accumulated amount of water, W_{total}, upwelled (or downwelled) by the meridional wind between the coast and the position x is finally transported offshore with the zonal Ekman transport. In this study, the integrals were carried out from the coast up to a point far offshore where the long-term average of wind stress curl equals zero (Fig. 1b).

Ocean dynamics is associated with many other flow elements, such as the formation of horizontal pressure gradients from upwelling, coastal jets, thermal fronts, sub-mesoscale instabilities, etc. (Fennel 1999; de Szoeke and Richman 1984; Abrahams et al., 2021). However, here the ocean consideration motivates the choice of the atmosphere variables, but the analysis stays entirely on the atmospheric drivers of upwelling and is independent of the simplifications made on the ocean side. We focus on three quantities representing the forcing of upwelling in the coastal ocean. The first quantity is the cross-shore integrated upwelling velocity (W_{total}). It is proportional to the meridional wind stress found offshore and is synonymously to the Ekman transport and approximates the total accumulated upwelling,

$$W_{total}(x) = -\frac{\tau^y(x)}{f\rho_w} = -U_E(x) \quad (7)$$

This quantity was previously analyzed by Lamont et al. (2018). The second and the third quantities are cross-shore integrated WSCD upwelling and coastal upwelling velocities, here referred to as W_{curl} and W_{coast}, respectively. These quantities are estimated as follows:

$$W_{curl} = -\frac{\tau^y(x)}{f\rho_w} + \frac{\tau^y(x=0)}{f\rho_w} \quad (8)$$

$$W_{coast} = -\frac{\tau^y(x=0)}{f\rho_w}.$$

For the total (integrated) amount of upwelled water, i.e., W_{total}, details of the spatial pattern of the wind over the coastal zones do not play a significant role. This is important for the coastal wind drop-off known to occur within a few 10-km coastal bands. It cannot be adequately resolved in the available data ERA5 and ASCAT data defined on a coarse (i.e., 0.25°x0.25°) grid. However, for both w_{curl} and w_{coast}, those details matter. Underestimation of the coastal wind results in underestimated w_{coast} and overestimated w_{curl} and vice versa. However, this issue does not play a significant role in W_{total}. A summary of the quantities used to estimate the variation of wind-driven upwelling is given in table 1.

https://doi.org/10.5194/esd-2023-10
Preprint. Discussion started: 25 April 2023

Earth System Dynamics
Discussions

Table 1: A summary of wind-driven upwelling related quantities used in this study. Positive values indicate upward velocity (i.e., upwelling) for all quantities.

Acronyms	Definition	Formula	Acronyms	Definition	Formula
W_{curl}	Cross-shore integral of wind stress curl-driven upwelling velocity	$-\frac{\tau^y(x)}{f\rho_w} + \frac{\tau^y(x=0)}{f\rho_w}$	w_{curl}	Wind stress curl-driven upwelling velocity	$\frac{1}{\rho_w f}\left(\frac{\partial \tau_y}{\partial x} - \frac{\partial \tau_x}{\partial y}\right)$
W_{coast}	Cross-shore integral of coastal upwelling velocity	$-\frac{\tau^y(x=0)}{f\rho_w}$	w_{coast}	Alongshore-driven coastal upwelling velocity	$\frac{-2\tau^y(x=0)}{f\rho_w}\frac{e^{\frac{2x}{R_1}}}{R_1}$
W_{total}	Cross-shore integral of total upwelling velocity	$-\frac{\tau^y(x)}{f\rho_w}$			

In this study, we use the nearest grid point to the coast for computing the W_{coast} and w_{coast}. We will discuss long time series of these quantities extracted for the Kunene, Walvis Bay, Lüderitz, and Cape Columbine upwelling cells.

To have a rough estimate of w_{coast} in the upwelling cells, we compute the maximum upwelling velocity (see equation 5). We used R_1 from Chelton et al. (1998) in the nearest grid point to the upwelling cells (Fig. S5). We also compute the WSCD upwelling in each grid point (Fig. 1).

Mid-latitude atmospheric dynamics are characterized by frontal passages and passing cyclones and anticyclones shifting the position of semi-permanent SAA every several days (Richter et al., 2008; Gilliland and Keim, 2017; Sun et al., 2017). To identify the SAA center, we use monthly mean SLP values to filter out rapidly-varying migrating anticyclones, cyclones, and fragmented pressure systems. We employ a straightforward approach in the previous study to estimate the mean position and intensity of SAA (Gilliland and Keim 2017). First, we calculated the spatial average of the monthly-mean SLP in the region between 40°W-20°E and 45°-10°S. In the next step, the grid points with SLPs smaller than the average were flagged. The spatial average was calculated again by excluding the flagged grid points. SLP values smaller than the mean were flagged again. This way, the maximum pressure center within the South Atlantic domain is likely obtained, and secondary local SLPs maxima are eliminated. From the remaining grid points, those with SLPs greater than one standard deviation above the average were chosen to compute the position and intensity of the SAA core. When more than one group of separated grid points exists, we considered that closer to the SAA's climatological position (Fig. S6). It is worth noting that the climatology of the SAA (Fig. S6) was based on the annual mean SLP. The applied methodology yielded only one maximum pressure center over the entire domain for all calendar months.

The intensity of the SAA is defined as the areal average of the SLP over the remaining grid points. Likewise, we compute the SAA's position (i.e., longitude, latitude). Multiple centers were observed only during 19 months out of 516 months. In general, the annual cycle of SLP reveals the SAA center in its northernmost and westernmost position during austral winter (i.e., Jun-Aug; Fig. S6). The SLP in the core of SAA varies seasonally from about 1020 hPa in February to about 1024.6 hPa in August.

We estimate the trend (α) in the SLP and the SAA position by using the least square linear regression method. The variability is estimated by the Standard deviation of yearly mean values (σ_{yr}) after subtracting the long-term linear

https://doi.org/10.5194/esd-2023-10
Preprint. Discussion started: 25 April 2023

Earth System Dynamics Discussions

trend. The importance of the long-term historical changes relative to fluctuations due to internal climate variability is estimated by the signal-to-noise ratio (S/N), which is computed as follows:

$$S/_N = \frac{\Delta}{2\sigma_{yr}} = \frac{\alpha \times T}{2\sigma_{yr}}, \quad (9)$$

where T stands for the time span of the ERA5 data set (i.e., 43 year) and Δ shows the changes associated with the long-term trend. In this way, a high S/N means a robust long-term change relative to the background noises (Bordbar et al., 2015, 2019). A small S/N indicates low confidence in the long-term trend.

To identify the connection between different quantities, we computed their linear correlation. To suppress the possibly misleading impacts of the seasonal cycle on the results, we subtracted the climatological monthly mean before calculating the correlation. This correlation is referred to as anomaly correlation (Reintges et al., 2020).

3 Results and discussions

The long-term average of W_{coast}, W_{curl}, and W_{total}, along with the spatial pattern of WSCD upwelling, are shown in Fig. 1. The long-term average of W_{coast} is positive (i.e., upwelling favorable) over the entire BUS. It features two pronounced peaks off the mouth of the Kunene river (~17.5°S) and Lüderitz (26.5°S). They are attributed to the local intensification of alongshore winds associated with the northward atmospheric low-level jet (Patricola and Chang, 2017). Almost over the entire domain, the long-term mean of W_{curl} is positive. The exception is a sector near the Kunene upwelling cell (~19.5°S to 17.5°S), which features downward transport (i.e., downwelling). This finding is consistent with previous studies (Fennel 1999; Bordbar et al., 2021). Off Walvis Bay, the mean of W_{curl} reaches its maximum. From north of Lüderitz (~25.5°S) to south of Cape Frio (~18.5°S), the long-term average of W_{curl} exceeds that for W_{coast}. Overall, the long-term mean W_{total} remains relatively invariant with latitude across the nBUS. In contrast, it is reduced southward in the sBUS (i.e., from Lüderitz to Cape Columbine). It is worth noting that in the sBUS surface wind undergoes seasonal reversal and upwelling is seasonal (Shannon 1985). The spatial pattern of WSCD upwelling features salient features of the BUS, such as equatorward widening of the BUS, and large WSCD upwelling off Walvis Bay, which is consistent with previous studies (Fennel 1999; Bordbar et al., 2021).

The monthly anomaly correlation coefficients of the SAA (i.e., intensity, longitude, and latitude) with W_{coast}, W_{curl}, W_{total}, and the WSCD upwelling are shown in Fig. 2 a-c. Note that the climatological monthly mean was subtracted in each time series before computing the correlation. The anomaly correlation of the SAA intensity with W_{coast}, W_{curl}, and W_{total} (Fig. 2a) reveals positive values, implying the intensified SAA is likely associated with enhanced upwelling across the entire BUS. The correlation for W_{total} exceeds 0.4 almost for all latitudes, which is more robust over the sBUS (green line in Fig. 2a). Our analysis indicates that robust changes in the intensity of the SAA, in general, affect the WSCD upwelling more than the alongshore wind-driven upwelling close to the coast. The anomaly correlation of W_{coast} with the SAA intensity is mostly weak (brown line in Fig. 2a). Within the most intense coastal upwelling cells in the BUS, the Kunene and Lüderitz upwelling cell, W_{coast} weakly correlates with the SAA intensity and the anomaly correlation with SAA position even vanishes. Almost over the entire domain, the anomaly correlation of W_{curl} with the SSA intensity (blue line in Fig. 2a) exceeds that for W_{coast}. The correlation coefficient for W_{curl} exceeds 0.4 from south of Cape Frio (~19°S) to north of Lüderitz (~25.5) and almost over the entire sBUS, whereas the correlation for W_{coast} hardly exceeds 0.4 throughout the BUS.

https://doi.org/10.5194/esd-2023-10
Preprint. Discussion started: 25 April 2023

Earth System Dynamics
Discussions

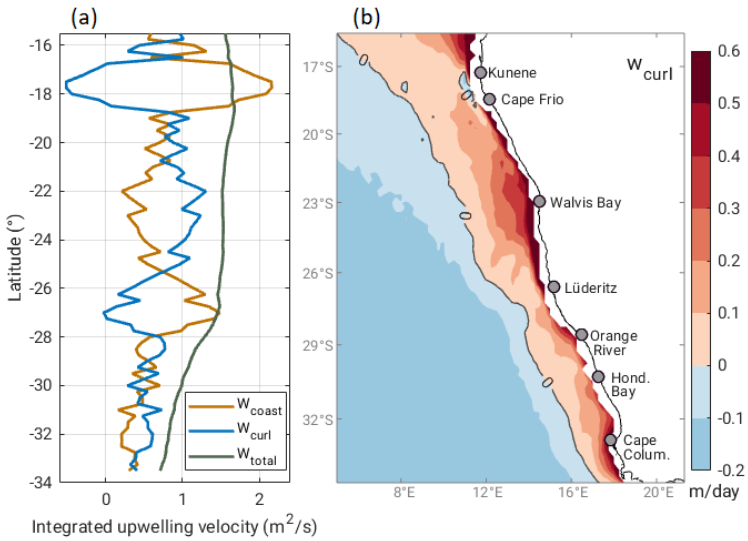

Figure 1: Long-term average of W_{coast}, W_{curl}, W_{total} (a; m^2/s), and spatial pattern of long-term average WSCD upwelling (b; m/d) across the BUS obtained from the ERA5 wind over 1979-2021. Contours in panel b indicates where the WSCD upwelling is equal to zero.

The anomaly correlation of W_{total}, W_{coast}, W_{curl} with the SAA longitude is weak (Fig. 2b). With regard to the SAA latitude (Fig. 2c), the correlation coefficient for W_{curl} and W_{total} is negative and smaller than -0.4 over the entire sBUS, meaning southward displacement of the SAA is associated with an enhanced W_{curl} and W_{total}. However, the correlation for W_{coast} is relatively weak. For the nBUS, these correlations are not statistically significant.

The anomaly correlation between the SAA intensity and the WSCD upwelling (Fig. 2d) is broadly positive across the entire BUS, meaning an intensification of SAA is likely associated with a strengthening of WSCD upwelling. Indeed, the spatial pattern of the correlation between the SAA intensity and the WSCD upwelling is reminiscent of the long-term average of the WSCD upwelling (Fig. 1), with an enhanced value off Walvis Bay and south of Lüderitz. This is consistent with the correlation between SAA intensity and W_{curl} (Fig. 2a). The WSCD upwelling anomaly in the sBUS appears to be significantly affected by the meridional displacement of the SAA (Fig. 2f). Generally, the SAA poleward excursion is likely resulting in an enhanced WSCD upwelling over the entire sBUS. In the whole BUS, the anomaly correlation between the WSCD upwelling and the SAA longitude is weak (Fig. 2e), which is consistent with the correlation between W_{curl} and the SAA longitude (Fig. 2b). Overall, these anomaly correlation patterns indicate that any of the SAA systematic changes have different consequences for the wind-driven upwelling in the nBUS and sBUS.

We ask for specific correlation patterns for the austral summer or winter months, corresponding to maximum or minimum solar radiation. Repeating the same analysis for the austral winter (Jun-Aug; Fig. S7) and summer (Dec-Feb; Fig. S8), the general structures of the anomaly correlations do not change much. Overall, the size of correlations is higher in the austral winter than in the austral summer. Wintertime W_{total} and the SAA intensity are closely connected, with the correlation coefficient is higher than 0.5 for most of the BUS. In sBUS, wintertime W_{total} and the SAA latitude are strongly anti-correlated, with a correlation coefficient smaller than -0.6. It suggests that the poleward excursion of the SAA in boreal winter is very likely associated with an enhanced W_{total} across the sBUS. Since the coastal upwelling undergoes a strong seasonal cycle south of the Lüderitz upwelling cell (~27°S), including the seasonal cycle in the correlation would yield a different pattern.

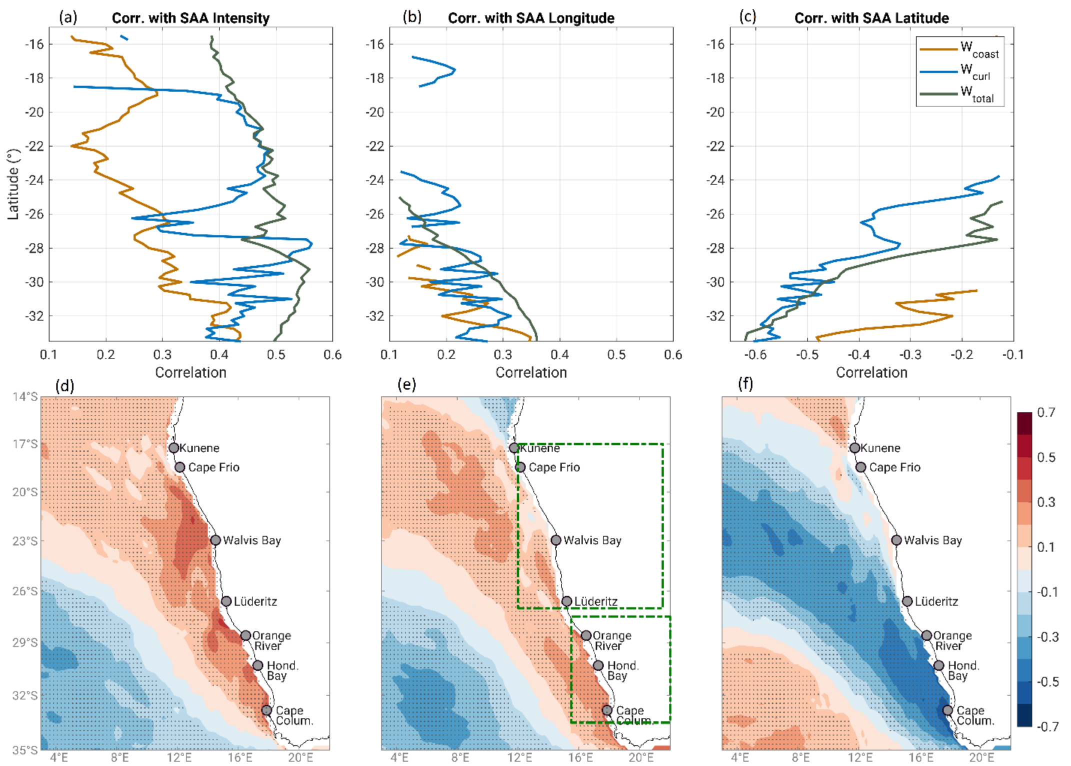

Figure 2: Monthly anomaly correlation of the SAA intensity (a), longitude (b), and latitude (c) with W_{coast} (brown line), W_{curl} *(blue line), and* W_{total} (green line) in each latitude across the BUS. Shown correlations in panel a-c are statistically significant at the 99% confidence level. The correlation of the WSCD upwelling with the intensity (d), longitude (e), and latitude (f) of the SAA are displayed in bottom panels. Stippled areas in d-f indicate where the correlation is statistically significant at the 99% confidence level.

We found the wind-driven upwelling in the BUS is significantly affected by the variations of the SAA. We also assess the changes in the regional horizontal pressure gradient, which determines geostrophic winds and have strong influence on the local winds (Lamont et al., 2018). The differences between the SLP over the SAA core and the areal-averaged SLPs over the nBUS and sBUS (Fig. 2e) are considered as approximation for the SLP gradient related to the surface wind regimes.

The time series of the SLP over the SAA and its contrast with the SLP in the nBUS and sBUS show marginal positive trends of about 0.020, 0.014, and 0.015 hPa/yr, respectively (Fig. 3a). But the interannual variation of the SLP is large and reduces confidence in the significance of the trend. The S/N of the trends is typically smaller than 1.0. The time series of the SLP gradients follow the SLP of the SAA core reasonably well, implying that the variability of the SLP gradients is largely related to the SAA. We repeated these analyses for different rectangular boxes and found that the trends of the SLP gradients were not sensitive to the size of rectangular boxes (not shown). There is a slight westward and poleward migration of the SAA of about -0.15°E, and -0.50°N degrees over the observation period of 43-year, respectively (Fig. 3b). The small S/N does not allow for a meaningful statement about the SAA long-term excursion. The time series of the SAA longitude shows a wide range of zonal SAA excursions between about 30°W and about 5°E. Several events with a large excursion of the SAA occurred every few years, i.e., on an interannual timescale, but sometimes an anomalous zonal displacement persisted for a few years. For example, the years 1997 and 2006 are characterized by persistent eastward SAA displacements, and the years 1986, 2001, 2010, and 2017 feature anomalous westward SAA migrations. The meridional position of the SAA ranges from 35°S to 25°S.

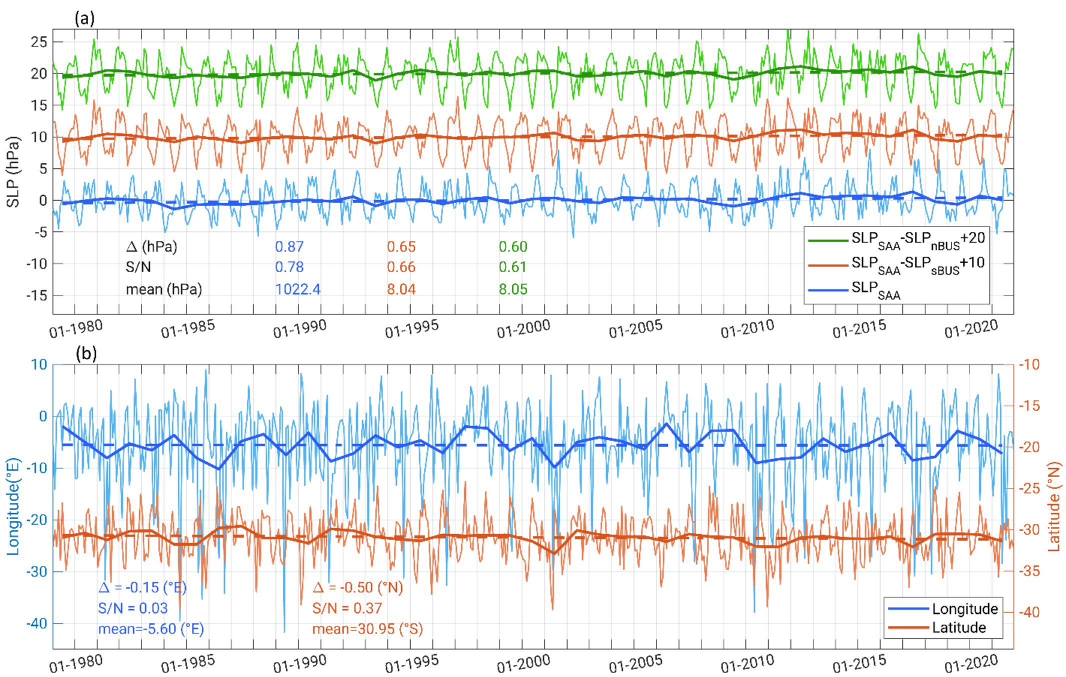

Figure 3: a, Time series of the SLP in the SAA core (blue lines) and its difference with the SLP over nBUS (green lines) and sBUS (red lines). The SLP for the nBUS and the sBUS is the average over the rectangular boxes displayed in Fig. 2 e. The long-term mean was subtracted from each time series. Please note the offsets for the nBUS (+10 hPa) and sBUS (+20hPa) time series. In panel (b), the time series of longitude (blue; °E) and latitude (red; °N) of the SAA core are shown. In both panels, thick solid lines and dashed lines denote the monthly and yearly mean, and the trend line fitted to the yearly mean values. At the bottom of each panel, the long-term changes associated with trend line (i.e., Δ), the corresponding S/N, and the mean are shown by identical colors as the time series.

We computed the SAA intensity and position time series for Jan-Feb and Jun-Aug, corresponding to austral summer and winter, respectively (Fig. S9). Again, a positive trend in the summertime and wintertime SAA intensity is found, but the corresponding S/N remains smaller than unity. Despite the steadily enhanced CO_2 emission since the 1990s (Smith et al., 2021) and the changes in the global heat budget, the SAA intensity and position remained steady and underwent no significant trend. It is consistent with the previous study (Polonsky & Serebrennikov, 2021), which

https://doi.org/10.5194/esd-2023-10
Preprint. Discussion started: 25 April 2023

Earth System Dynamics
Discussions

reported a hiatus in the intensification of the coastal upwelling across the BUS since the 1990s. If there is any tendency due to the enhanced radiative forcing, it is presumably hidden by the internal climate variability.

To investigate this further, the long-term trend in the yearly, Jul-Oct, and Jan-Apr SLP means are shown in Fig. 4. The SLP trend appears to be positive almost over the entire South Atlantic. However, the pattern of rising SLP is not uniform, and the maximum trend is not found in the SAA center. The positive trend is more prominent over higher latitudes, particularly for July-October. The most prominent trend is found in the southwest and the southeast of the domain in Jul-Oct (Fig. 4c) and Jan-Apr (Fig. 4b), respectively. The structure of the trend reminds the recent multi-decadal trend in the SAM, which is associated with an enhanced meridional SLP gradient between the polar and mid-latitudes (Wachter et al., 2020; Fogt & Marshall, 2020). The SLP trend over the center of SAA is about 0.02 hPa/yr (i.e., Δ of ~0.86 hPa) and larger than that near the coast of Namibia and South Africa. It indicates a slight enhancement of the SLP gradients between the SAA and the BUS coastal zones. This enhanced SLP gradient appears to be slightly more (less) pronounced for the Jul-Oct (Jan-Apr) historical changes (Fig. 4b, c).

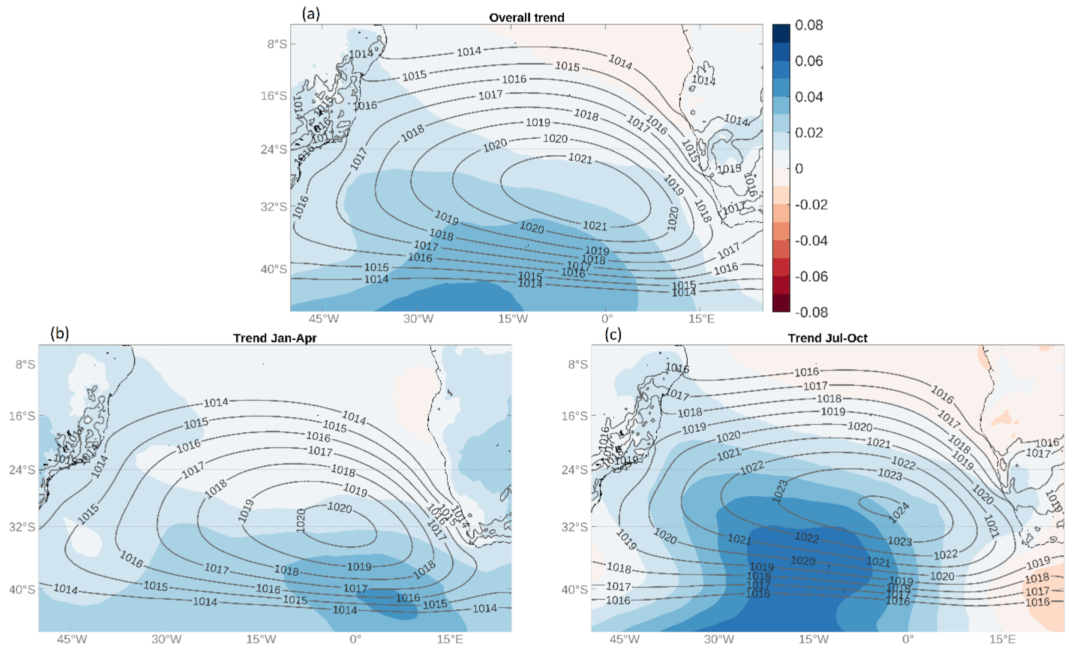

Figure 4: Long-term mean (contours; hPa) and trend (color shading; hPa/yr) of the ERA5 SLP for 1979-2021. Panel (a) represents the trend (*α*) and mean-state obtained over the entire calendar months, whereas (b-c) corresponds to the averages over Jan-Apr and Jul-Oct, respectively.

In Fig. 5, the variability (i.e., σ_{yr}) of the SLP and the S/N of the long-term SLP trends are displayed. The S/N indicates whether the long-term trend can emerge from the fluctuations associated with internal climate variability. Internal climate variability is enhanced poleward across the entire domain (contours in Fig. 5). The SLP variability in the southern sector is more than twice that in the north and central parts. The year-to-year variations are considerable for the wintertime when the region's meridional SST gradient reaches its seasonal maximum. Further, severe cyclones, anticyclones, and frontal passages are more frequent during wintertime. For the yearly mean SLP (Fig. 5a), the S/N

https://doi.org/10.5194/esd-2023-10
Preprint. Discussion started: 25 April 2023

barely exceeds 1. An exception is an area between 40°-35°S and 15°W-5°W with S/N of about 1.3. Small S/N highlights that the historical trends do not come to light in the presence of strong internal climate variability. For both, winter- and summertime historical trends the S/N remains smaller than one over almost the entire domain, (Fig. 5b,c). Hence, the long-term SLP trends should be interpreted with caution. The time series of the SAA intensity and its geographic position further supports this result (Fig. 3, Fig. S9).

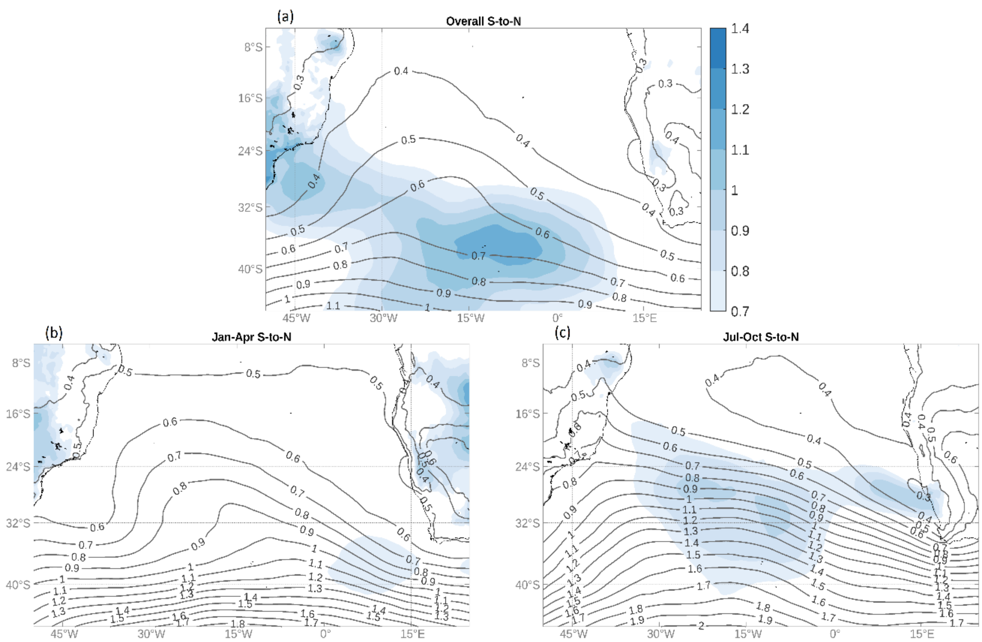

Figure 5: Spatial pattern of the variability (i.e., σ_{yr}; contours; hPa) and signal-to-noise ratio (S/N) associated with the long-term trend (color shading) of the ERA5 SLP over 1979-2021. Panel (a) represents the values obtained over the entire calendar year, whereas panels (b) and (c) correspond to the average over Jan-Apr and Jul-Oct, respectively.

In the following, we further assess the historical changes of W_{coast} and W_{curl} in four upwelling cells, including Kunene, Walvis Bay, Lüderitz, and Cape Columbine (Fig. 6-8). In the Kunene cell, positive W_{coast} (i.e., upwelling favorable) persists throughout the year (Fig. 6a, 8a). The annual mean W_{coast} is around 1.96 m^2/s. The related maximum upwelling velocity approximated by using equation 5 (see methods) is roughly 6.9 m/d, which is one order of magnitude larger than the typical size of WSCD upwelling (i.e., w_{curl}) across the BUS (see Fig. 1b). The distribution of W_{coast} in Kunene cell is skewed towards strong upward transport and exhibits interannual variability. In addition, the number of severe W_{coast} indicated by outliers remains nearly steady over the considered period. Compared with that of W_{coast}, the distribution of W_{curl} in Kunene cell has smaller skewness (Fig. 7a). Unlike W_{coast}, W_{curl} is not perennial. It also undergoes a strong interannual variability. The number of days with positive W_{curl} in a year varies from 110 to 160 (Fig. 8b). Outliers in W_{curl} appeared almost every year.

Off Walvis Bay, the mean of W_{coast} is about 0.35 m^2/s. Based on equation 5, upwelling velocity is roughly 2.0 m/d. Negative W_{coast} (i.e., downwelling favorable) appeared more frequently off Walvis Bay than in the Kunene upwelling

https://doi.org/10.5194/esd-2023-10
Preprint. Discussion started: 25 April 2023

Earth System Dynamics
Open Access
Discussions

cell (Fig. 6b). However, the number of days with positive W_{coast} off Walvis Bay remains higher than 300 per year (Fig. 8c). Since the late 1990s, there has been a slight trend toward stronger W_{coast}, with several vigorous upwelling events that can be considered as anomalous events. A large interannual variation in W_{coast} off Walvis Bay is visible. Persisting throughout the year, positive W_{curl} off Walvis Bay is the strongest among the upwelling cells (Fig. 7b, 8d). The number of days with the upwelling-favorable W_{curl} is higher than 340 per year in the Walvis Bay upwelling cell. This number remained steady with no significant trend.

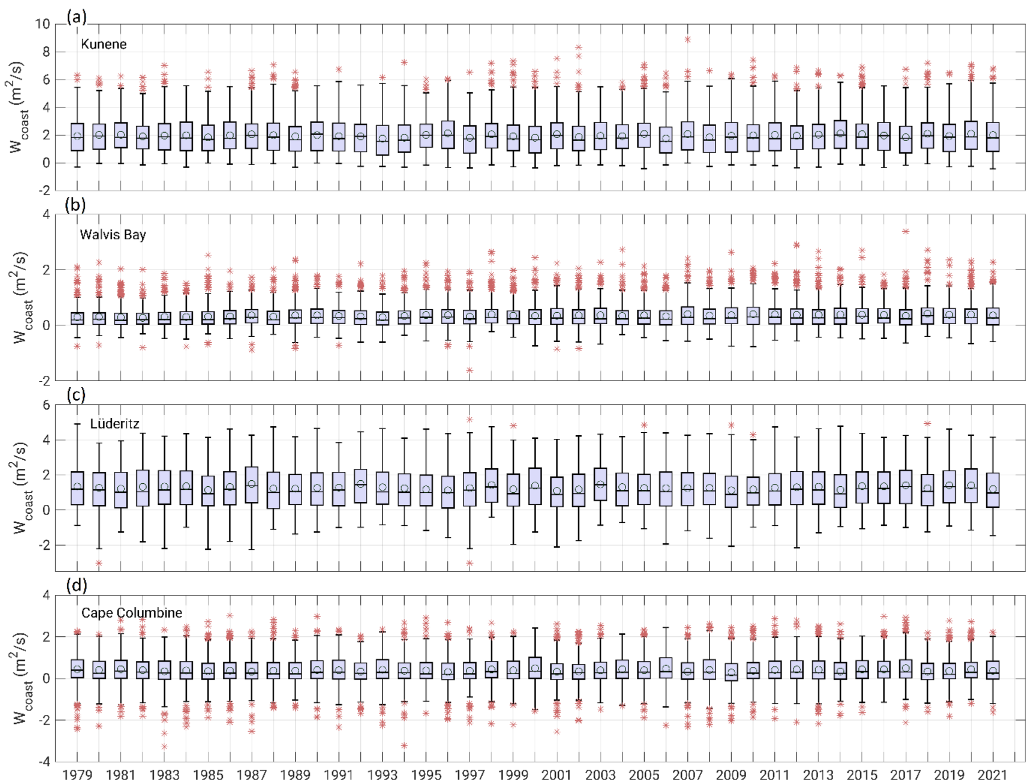

Figure 6: Boxplot representing the median and the interquartile range of W_{coast} in Kunene (a), Walvis Bay (b), Lüderitz (c), and Cape Columbine (d) upwelling cells derived from ERA5 data over 1979-2021. Each box represents the distribution of the daily W_{coast} in the corresponding year. The bands and circles inside the boxes represent the medians and mean, respectively. The red crosses indicate the extreme events defined as the values exceeding the confidence limits (i.e., outliers). W_{coast} for the Kunene, Walvis Bay, Lüderitz, and Cape Columbine are the average over 17.5°S-17°S, 23.5°S-23°S, 27°S-26.5°S, and 33.25°S-32.75°S, respectively.

Within the Lüderitz cell (Fig. 6c, 8e), positive W_{coast} is almost year-round, with a long-term mean of about 1.28 m^2/s. Based on equation 5, this corresponds to an upwelling velocity of about 6.9 m/d. The positive W_{coast} occurred at more than 300 days in a year (Fig. 6c, 8e). However, there are also episodes with negative W_{coast}. Only a few outliers in W_{coast} off Lüderitz (e.g., 2005, 2009, 2010, 2018) were observed. In contrast, outliers in W_{curl} off Lüderitz are observed almost every year (Fig. 7c). The number of days with positive W_{curl} fluctuates around 220 per year (Fig. 8f).

https://doi.org/10.5194/esd-2023-10
Preprint. Discussion started: 25 April 2023

Earth System Dynamics
Discussions

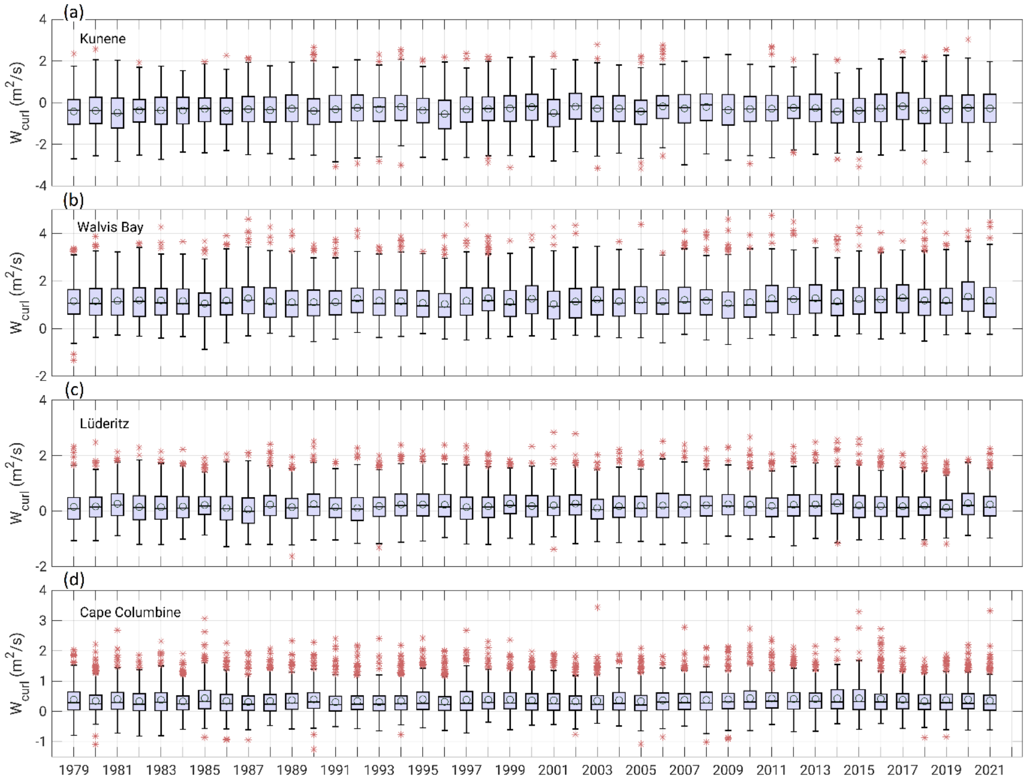

Figure 7: Boxplot representing the median and the interquartile range of W_{curl} in Kunene (a), Walvis Bay (b), Lüderitz (c), and Cape Columbine (d) upwelling cells derived from ERA5 data over 1979-2021. Each box represents the distribution of the daily W_{curl} in the corresponding year. The bands and circles inside the boxes represent the medians and mean, respectively. The red crosses indicate the extreme events defined as the values exceeding the confidence limits (i.e., outliers). W_{curl} for the Kunene, Walvis Bay, Lüderitz, and Cape Columbine are the average over 17.5°S-17°S, 23.5°S-23°S, 27°S-26.5°S, and 33.25°S-32.75°S, respectively.

Off Cape Columbine, the seasonal reversal in W_{coast} is more pronounced than in other upwelling cells (Fig. 6d). The long-term mean of W_{coast} is about 0.39 m^2/s. Based on equation 5, the maximum upwelling velocity is about 2.5 m/d. The number of days with positive W_{coast} is around 270 per year (Fig. 8g). W_{coast} does not show a long-term trend but undergoes interannual variability. As for W_{curl} (Fig. 7d), outliers are primarily positive. The days with positive W_{curl} fluctuate around 300 per year (Fig. 8h).

In all upwelling cells over the considered time span, there is no robust trend in the strength and variability of W_{coast} and W_{curl}. However, the time series are not sufficiently long to identify a potential impacts of modes of climate variability, such as the SAM, the Interdecadal Pacific Oscillation, and Atlantic Multidecadal Variability, which all span variability on decadal timescales and beyond.

https://doi.org/10.5194/esd-2023-10
Preprint. Discussion started: 25 April 2023

Earth System Dynamics
Discussions

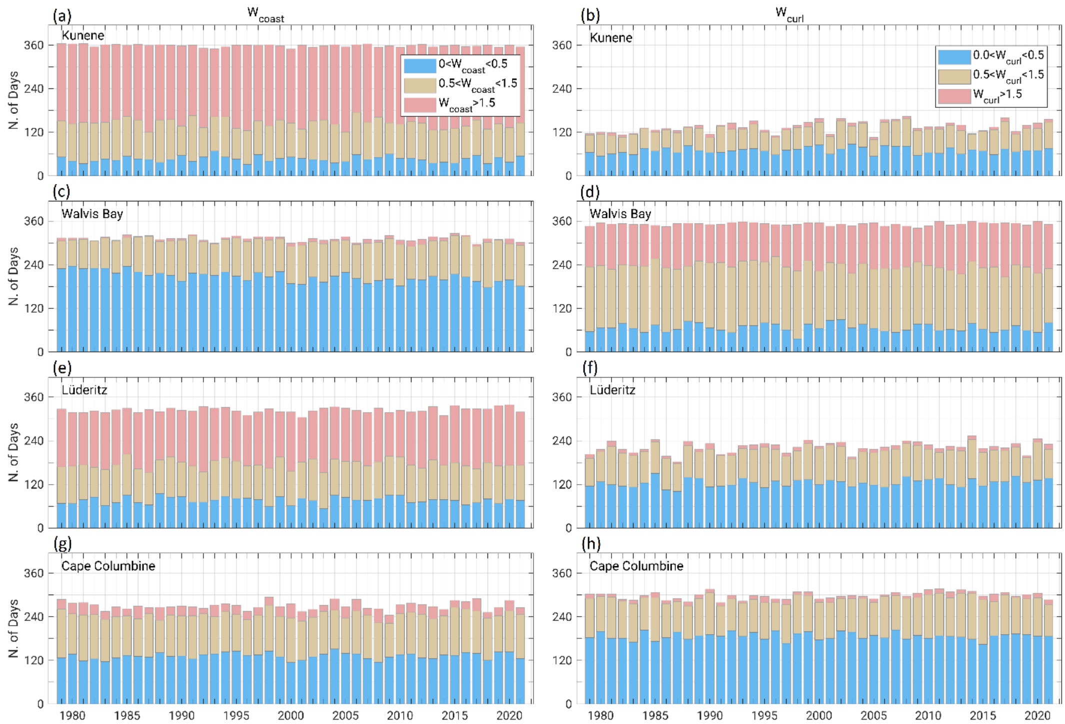

Figure 8: Number of days per year with upwelling favorable W_{coast} (a,c,e,g) and W_{curl} (b,d,f,h) in Kunene (a,b), Walvis Bay (c,d), Lüderitz (e,f), and Cape Columbine (g,h). Light blue, light yellow, and light red bars indicate weak ($0.0<W<0.5\ m^2/s$), moderate ($0.5<W<1.5\ m^2/s$), and strong ($W>1.5\ m^2/s$) transport.

4 Summary

To get new insight into the multi-decadal variation of the South Atlantic Anticyclone (SAA) and its link to the wind-driven upwelling across the Benguela Upwelling System (BUS), the observed sea level pressure (SLP) and surface wind datasets from ERA5 archive were analyzed. Here, we considered the cross-shore integral of wind-driven coastal upwelling (W_{coast}), the wind stress curl-driven upwelling (W_{curl}), and their summation (W_{total}). The detail structure of the wind over the coastal zones plays a significant role in local wind-driven coastal upwelling and wind stress curl-driven upwelling. However, we show that the detailed wind pattern over the coastal zone does not play a significant role for W_{total}. Since it provides an accurate estimate of W_{total}, this approach is promising and suitable for the ERA5 data, even though the resolution of this data is too coarse (i.e., 0.25°x0.25°) to resolve coastal wind drop-off.

We found a robust anomaly correlation between the SAA intensity, W_{total}, and W_{curl} over almost the entire BUS. However, this correlation for W_{coast} is much weaker. An intensified SAA is likely accompanied by an enhanced W_{total} and W_{curl}. For W_{total}, this connection seems to be more pronounced in the poleward sector of the BUS. For W_{curl}, the relationship with the SAA intensity is most robust off Walvis Bay and south of the Lüderitz upwelling cell, which feature a larger W_{curl} long-term mean relative to the rest of the BUS. Further, a southward SAA excursion is likely associated with strengthening W_{total} and W_{curl} over the poleward portion of the BUS. This connection is more pronounced during austral winter (i.e., June-August). Our findings suggest that robust changes in the SAA (i.e., intensity and position) affect the wind stress curl-driven upwelling more than the alongshore wind-driven coastal upwelling in the BUS. Thus, any systematic changes in the SAA can have different implications across the Benguela ecosystems.

Despite a slight upward SLP trend in the subtropical South Atlantic, the ratio between historical changes associated with the trend and the changes due to internal climate variability is small. Also, wind-driven upwelling in several upwelling cells remained steady and exhibited neither a significant long-term trend nor changes in the characteristics of the variability (i.e., period and amplitude). It suggests that the historical trends in the SLP and wind-driven upwelling during 1979-2021 do not come to light in the presence of internal climate variability. If there is any human-caused signal in the SAA, it has been confounded by internal variability.

The analyzed ERA5 data sets are presumably too short for detecting the regional wind-driven upwelling systematic changes associated with global warming. Hence, it remains difficult to examine Bakun's hypothesis reliably. Indeed, one cannot attribute the entire wind field variability over the BUS solely to the SAA and the regional cross-shore surface air temperature gradient. Localized drivers of the surface winds (e.g., sub-mesoscale fronts, eddies, and land-sea breezes), which the operational model used in ERA5 reanalysis does not resolve, may significantly alter the surface wind field. Furthermore, one should not neglect the internally and externally forced variations of the key components of the general atmospheric circulation (i.e., the Hadley Cell, the Walker Circulation) and their potential impacts on the SAA and the surface winds across the BUS (Gillett et al., 2006; Gilliland & Keim, 2017; Rouault & Tomety, 2022).

It is worth noting that the enhanced ocean stratification is a well-established consequence of ocean warming, suppressing the upwelling efficacy in nutrient supply. Thus, an intensified upwelling-favorable wind does not necessarily imply an enhanced nutrient availability in the euphotic zones.

The analysis conducted in this study is broadly transferrable to other major Eastern Boundary Upwelling Systems and will be beneficial for regional marine ecosystem studies.

Data availability. ERA5 SLP and surface wind (Hersbach et al., 2018) were obtained from https://cds.climate.copernicus.eu. ASCAT surface winds (Ricciardulli and Wentz, 2016) were downloaded from https://remss.com/missions/ascat/. Observed SLP in the St. Helena Island (Feistel et al., 2003) can be publically accessed at https://www.io-warnemuende.de/hix-st-helena-island-climate-index.html.

Author contributions. MHB, MSCH, and VM developed the methodology and contributed to interpreting the results, discussion, and refinement of the paper. MHB wrote the first draft of the paper.

Conflicts of Interests. The authors declare no conflict of interest.

Acknowledgements. This study was conducted within the frame of the EVAR and BANINO project sponsored by the BMBF with the reference number 03F0814, and 03F0795B, respectively. This study has been conducted using E.U. Copernicus Marine Service Information.

References

Abrahams, A., Schlegel, R. W., and Smit, A. J.: Variation and change of upwelling dynamics detected in the world's eastern boundary upwelling systems. Frontiers in Marine Science, 8, p.626411, 2021.

https://doi.org/10.5194/esd-2023-10
Preprint. Discussion started: 25 April 2023

Earth System Dynamics
Discussions

Abrahams, A., Schlegel, R. W., and Smit, A. J.: A novel approach to quantify metrics of upwelling intensity, frequency, and duration. PLoS One, 16(7), p.e0254026, 2021.

Bakun, A.: Global climate change and intensification of coastal ocean upwelling. Science, 247(4939), pp.198-201, 1990.

Belmonte Rivas, M., and Stoffelen, A.: Characterizing ERA-Interim and ERA5 surface wind biases using ASCAT. Ocean Science, 15(3), pp.831-852, 2019.

Bettencourt, J. H., López, C., and Hernández-García, E.: Oceanic three-dimensional Lagrangian coherent structures: A study of a mesoscale eddy in the Benguela upwelling region. Ocean Modell., 51, 73–83, https://doi.org/10.1016/j.ocemod.2012.04.004, 2012.

Bonino, G., Di Lorenzo, E., Masina, S., and Iovino, D.: Interannual to decadal variability within and across the major Eastern Boundary Upwelling Systems. Scientific reports, 9(1), pp.1-14, 2019.

Bordbar, M. H., Martin, T., Latif, M., and Park. W.: Effects of long-term variability on projections of twenty-first century dynamic sea level. Nature Climate Change, 5(4), pp.343-347, 2015.

Bordbar, M. H., England, M. H., Sen Gupta, A., Santoso, A., Taschetto, A., Martin, T., Park, W., and Latif, M.: Uncertainty in near-term global surface warming linked to tropical Pacific climate variability. Nature communications, 10(1), pp.1-10, 2019.

Bordbar, M. H., Mohrholz, V., and Schmidt, M.: The relation of wind-driven coastal and offshore upwelling in the Benguela Upwelling System. Journal of Physical Oceanography, 51(10), pp.3117-3133, 2021.

Chelton, D. B., DeSzoeke, R. A., Schlax, M. G., El Naggar, K., and Siwertz, N.: Geographical variability of the first baroclinic Rossby radius of deformation. Journal of Physical Oceanography, 28(3), 433-460, 1998.

Ekman, V. W.: On the influence of the Earth's rotation on ocean-currents. Ark. Mat. Astron. Fys., 2, 1–52, 1905.

Feistel, R., Hagen, E., and Grant, K.: Climatic changes in the subtropical Southeast Atlantic: The St. Helena Island climate index (1893–1999). Progress in Oceanography, 59(2-3), pp.321-337, https://doi.org/10.1016/j.pocean.2003.07.002, 2003.

Fennel, W.: Theory of the Benguela upwelling system. J. Phys. Oceanogr., 29, 177–190, https://doi.org/10.1175/1520-0485(1999), 1999.

Fennel, W., and Lass, H. U.: On the impact of wind curls on coastal currents. J. Mar. Syst., 68, 128–142, 2007.

Fogt, R. L., and Marshall, G. A.: The Southern Annular Mode: variability, trends, and climate impacts across the Southern Hemisphere. Wiley Interdisciplinary Reviews: Climate Change, 11(4), e652, 2020.

Gill, A. E.: Atmosphere-Ocean Dynamics. International Geophysics Series, Vol. 30, Academic Press, 662 pp, 1982.

Gillett, N. P., Kell, T. D., and Jones, P. D.: Regional climate impacts of the Southern Annular Mode. Geophysical Research Letters, 33(23), 2006.

Gilliland, J. M., and Keim, B. D.: Position of the South Atlantic Anticyclone and its impact on surface conditions across Brazil. Journal of Applied Meteorology and Climatology, 57(3), pp.535-553, 2018.

Hersbach, H., Bell, B., Berrisford, P., Biavati, G. et al.: ERA5 hourly data on pressure levels from 1979 to present. Copernicus climate change service (c3s) climate data store (cds), 10, https://cds.climate.copernicus.eu/cdsapp#!/dataset/reanalysis-era5-single-levels, 2018.

https://doi.org/10.5194/esd-2023-10
Preprint. Discussion started: 25 April 2023

Hösen, E., Möller, J., Jochumsen, K., and Quadfasel, D.: Scales and properties of cold filaments in the Benguela upwelling system off Lüderitz. J. Geophys. Res. Oceans, 121, 1896–1913, https://doi.org/10.1002/2015JC011411, 2016.

Imbol Koungue, R. A., Rouault, M., Illig, S., et al.: Benguela Niños and Benguela Niñas in Forced Ocean Simulation From 1958 to 2015. J. Geophys. Res. Oceans 124:5923-5951. https://doi.org/10.1029/2019jc015013, 2019.

Johnson, J. A.: Modifications of coastal currents and upwelling by offshore variations in wind stress. Tellus, 28, 254–260, https://doi.org/10.3402/tellusa.v28i3.10287, 1976.

Junker, T., Mohrholz, V., Siegfried, L., and van der Plas, A.: Seasonal to interannual variability of water mass characteristics and currents on the Namibian shelf. J. Mar. Syst., 165, 36–46, 2017.

Kainge, P., Kirkman, S. P., Estevao. V. et al.: Fisheries yields, climate change, and ecosystem-based management of the Benguela Current Large Marine Ecosystem. Environmental Development 36:100567, 2020.

Kidson, J. W.: Interannual variations in the Southern Hemisphere circulation. J. of Climate, 1(12), 1177-1198, 1988.

Lamont, T., García-Reyes, M., Bograd, S. J., Van Der Lingen, C.D., and Sydeman, W. J.: Upwelling indices for comparative ecosystem studies: Variability in the Benguela Upwelling System. Journal of Marine Systems, 188, pp.3-16, 2018.

Lamont, T., Barlow, R. G., and Brewin, R. J.: Long-term trends in phytoplankton chlorophyll a and size structure in the Benguela upwelling system. J. Geophys. Res. Oceans, 124, 1170–1195, https://doi.org/10.1029/2018JC014334, 2019.

Lass, H. U., and Mohrholz, V.: On the interaction between the subtropical gyre and the subtropical cell on the shelf of the SE Atlantic. J. Mar. Syst., 74, 1–43, 2008.

Latif, M., Martin, T., Park, W., and Bordbar, M. H.: Internal Southern Ocean Centennial Variability: Dynamics, Impacts and Implications for Global Warming. In Climate Change: Multidecadal and Beyond (pp. 109-124), 2016.

Li, X., Bordbar, M. H., Latif, M., Park, W., and Harlaß, J.: Monthly to seasonal prediction of tropical Atlantic sea surface temperature with statistical models constructed from observations and data from the Kiel Climate Model. Climate Dynamics, 54(3), pp.1829-1850, 2020.

Narayan, N., Paul, A., Mulitza, S., and Schulz, M.: Trends in coastal upwelling intensity during the late 20th century. Ocean Science, 6(3), pp.815-823, 2010.

Patricola, C. M., and Chang, P.: Structure and dynamics of the Benguela low-level coastal 1004 jet. Climate Dynamics, 49, 2765-2788, 2017.

Pauly, D., and Christensen, V.: Primary production required to sustain global fisheries. Nature, 374(6519), pp.255-257, 1995.

Polonsky, A. B., and Serebrennikov, A. N.: Long-Term Tendencies of Intensity of Eastern Boundary Upwelling Systems Assessed from Different Satellite Data. Part 1: Atlantic Upwellings. Izvestiya, Atmospheric and Oceanic Physics, 57(12), pp.1658-1669, 2021.

Reintges, A., Latif, M., Bordbar, M. H., and Park, W.: Wind stress-induced multiyear predictability of annual extratropical North Atlantic Sea surface temperature anomalies. Geophysical Research Letters, 47(14), p.e2020GL087031, 2020.

https://doi.org/10.5194/esd-2023-10
Preprint. Discussion started: 25 April 2023

Ricciardulli, L., and Wentz, F. J.: Remote sensing systems ASCAT C-2015 daily ocean vector winds on 0.25 deg grid, version 02.1. Remote Sensing Systems, accessed 1 June 2019, http://www.remss.com/missions/ascat, 2016.

Richter, I., Mechoso, C. R., and Robertson, A. W.: What determines the position and intensity of the South Atlantic anticyclone in austral winter? An AGCM study. Journal of climate, 21(2), pp.214-229, 2008.

Rouault, M., and Tomety, F. S.: Impact of the El Niño Southern Oscillation on the Benguela upwelling. J. of Physical Oceanography, 52, 2573–2587, 2022.

Rykaczewski, R. R., and Checkley, D. M.: Influence of ocean winds on the pelagic ecosystem in upwelling regions. Proceedings of the National Academy of Sciences, 105(6), pp.1965-1970, 2008.

Rykaczewski, R., Dunne, J. P., Sydeman, W. J., García-Reyes, M., Black, B. A., and Bograd, S. J.: Poleward displacement of coastal upwelling-favorable winds in the ocean's eastern boundary currents through the 21st century. Geophysical Research Letters, 42(15), pp.6424-6431, 2015.

Shannon, L. V.: The Benguela ecosystem. Part I: Evolution of the Benguela, physical features and processes. Oceanogr. Mar. Biol., 23, 105–182, 1985.

Shannon, L. V., Boyd, A. J., Brundrit, G. B., et al.: On the Existence of an El-Niño-Type Phenomenon in the Benguela System. Journal of Marine Research 44:495-520, 1986.

Shannon, L. V., and Nelson, G.: The Benguela: large scale features and processes and system variability. The South Atlantic, pp. 163-210. Springer, Berlin, Heidelberg, 1996.

Smith, C. J., Harris, G. R., Palmer, M. D., et al.: Energy budget constraints on the time history of aerosol forcing and climate sensitivity. Journal of Geophysical Research: Atmospheres, 126(13), p.e2020JD033622, 2021.

Sun, X., Cook, K. H., and Vizy, E. K.: The South Atlantic subtropical high: climatology and interannual variability. Journal of Climate, 30(9), pp.3279-3296, 2017.

Sydeman, W. J., García-Reyes, M., Schoeman, et al.: Climate change and wind intensification in coastal upwelling ecosystems. Science, 345(6192), pp.77-80, 2014.

de Szoeke, R. A., and Richman, R.: On wind-driven mixed layers with strong horizontal gradients—A theory with application to coastal upwelling. J. Phys. Oceanogr., 14, 364–377, 1984.

Tim, N., Zorita, E., and Hünicke, B.: Decadal variability and trends of the Benguela Upwelling System as simulated in a high-resolution ocean simulation. Ocean science, 11, 483-502, 2015.

Wachter, P., Beck, C., Philipp, A., Höppner, K., and Jacobeit, J.: Spatiotemporal variability of the Southern Annular Mode and its influence on Antarctic surface temperatures. Journal of Geophysical Research: Atmospheres, 125(23), e2020JD033818, 2020.

Yoshida, K.: A theory of the Cromwell Current (the equatorial undercurrent) and of equatorial upwelling. J. Oceanogr. Soc. Jap., 15, 159-170, 1959.